SANDIA REPORT
SAND2009-6051
Unlimited Release
Printed September 2009

Advanced Fuel Chemistry for Advanced Engines

Craig A. Taatjes, James A. Miller, Judit Zádor, Ravi X. Fernandes, Leonard E. Jusinski

Prepared by
Sandia National Laboratories
Albuquerque, New Mexico 87185 and Livermore, California 94550

Sandia is a multiprogram laboratory operated by Sandia Corporation,
a Lockheed Martin Company, for the United States Department of Energy's
National Nuclear Security Administration under Contract DE-AC04-94AL85000.

Issued by Sandia National Laboratories, operated for the United States Department of Energy by Sandia Corporation.

Available to DOE and DOE contractors from
U.S. Department of Energy
Office of Scientific and Technical Information
P.O. Box 62
Oak Ridge, TN 37831

Telephone: (865) 576-8401
Facsimile: (865) 576-5728
E-Mail: reports@adonis.osti.gov
Online ordering: http://www.osti.gov/bridge

Available to the public from
U.S. Department of Commerce
National Technical Information Service
5285 Port Royal Rd.
Springfield, VA 22161

Telephone: (800) 553-6847
Facsimile: (703) 605-6900
E-Mail: orders@ntis.fedworld.gov
Online order: http://www.ntis.gov/help/ordermethods.asp?loc=7-4-0#online

SAND2009-6051
Unlimited Release
Printed September 2009

Advanced Fuel Chemistry for Advanced Engines

Craig A. Taatjes, James A. Miller, Judit Zádor, Ravi X. Fernandes, Leonard E. Jusinski
Combustion Chemistry and Diagnostics Department
Sandia National Laboratories
P.O. Box 969, MS 9055
Livermore, California 94550

Abstract

Autoignition chemistry is central to predictive modeling of many advanced engine designs that combine high efficiency and low inherent pollutant emissions. This chemistry, and especially its pressure dependence, is poorly known for fuels derived from heavy petroleum and for biofuels, both of which are becoming increasingly prominent in the nation's fuel stream. We have investigated the pressure dependence of key ignition reactions for a series of molecules representative of non-traditional and alternative fuels. These investigations combined experimental characterization of hydroxyl radical production in well-controlled photolytically initiated oxidation and a hybrid modeling strategy that linked detailed quantum chemistry and computational kinetics of critical reactions with rate-equation models of the global chemical system. Comprehensive mechanisms for autoignition generally ignore the pressure dependence of branching fractions in the important alkyl + O_2 reaction systems; however we have demonstrated that pressure-dependent "formally direct" pathways persist at in-cylinder pressures.

ACKNOWLEDGMENTS

We thank Dr. Ahren Jasper (8353) for assistance in quantum chemistry and fundamental computational kinetic methods; Dr. David Osborn (8353) and Dr. John T. Farrell (ExxonMobil) for assistance in the design of the high-pressure MBMS reactor. We also thank Prof. Giovanni Meloni (University of San Francisco) for his contributions to the experimental investigations.

CONTENTS

FIGURES

NOMENCLATURE

ALS	Advanced Light Source
B3LYP	Becke 3-parameter exchange, Lee, Yang and Parr
CASPT2	Complete active space with second-order perturbation theory
CBS	Complete basis-set extrapolation
DFT	Density-functional theory
DOE	Department of Energy
HCCI	Homogeneous-charge compression ignition
JBEI	Joint Bioenergy Institute
LBNL	(Ernest Orlando) Lawrence Berkeley National Laboratory
LIF	Laser-induced fluorescence
LTC	Low-temperature combustion
MAWP	Maximum allowable working pressure
MBMS	Molecular beam mass sampling
ME	Master equation
MRCI	Multireference configuration interaction
NO_x	Nitrogen oxides
QCISD(T)	Quadratic configuration interaction with single and double excitations and perturbative treatment of triple excitations
QOOH	(Substituted) hydroperoxyalkyl radical
R	(Substituted) alkyl radical
RO_2	(Substituted) alkylperoxy radical
RQCISD(T)	Restricted QCISD(T)
RRKM	Rice-Ramsperger-Kassel-Marcus
SNL	Sandia National Laboratories
TST	Transition-state theory
VRC-TST	Variable reaction coordinate transition-state theory
VTST	Variational transition-state theory

1. INTRODUCTION

The relationship of fuel chemistry to ignition is a centrally important knowledge area for predictive modeling of emerging low-temperature combustion (LTC) engines that promise to combine increased efficiency with low pollutant emission. Unlike traditional gasoline or diesel engines, where ignition timing is controlled by a spark or fuel injection, many advanced engine technologies rely on chemical kinetics to time a volumetric ignition and reaction process (Figure 1). However, the present understanding of this chemistry is inadequate; a critical deficiency for optimization of fuel-engine combinations is our ignorance of the detailed effects of fuel structure on ignition. Furthermore the dependence of the low temperature (< 800 K) oxidation reactions on the total pressure is not completely understood even for traditional hydrocarbon fuels; for example the highly successful model for isooctane combustion [1] fails to reproduce the response of compression-ignition operation to increased boost [2].

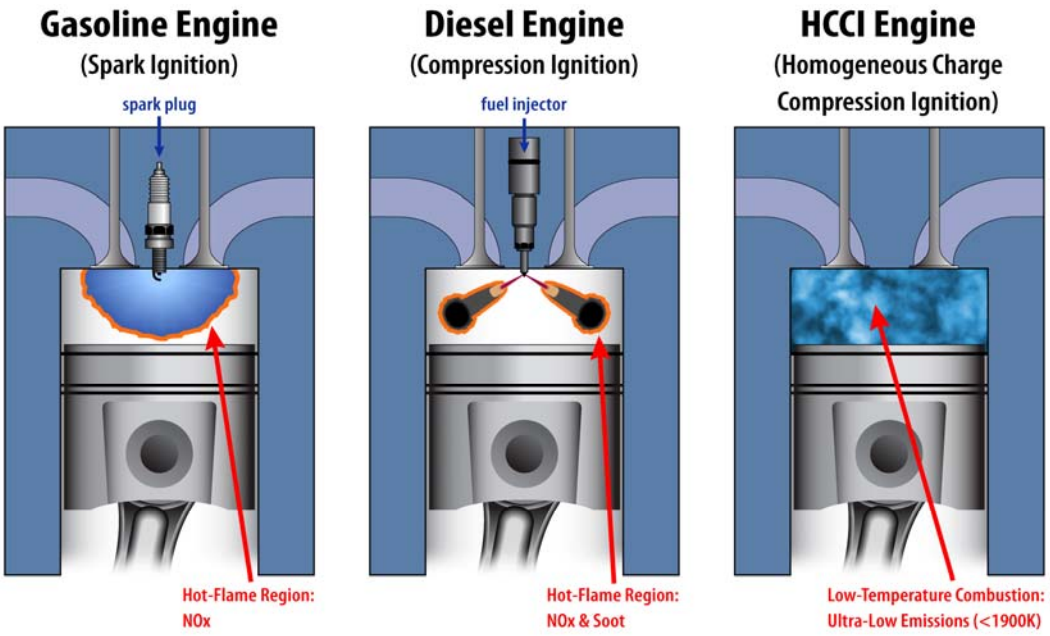

Figure 1. Schematic picture of combustion in traditional and advanced engines

New experimental and computational tools are required to successfully investigate the fuel-structure and pressure dependence of key chemical pathways in autoignition. Knowledge of this chemistry is central to engineering these advanced combustion technologies for a changing fuel stream, including biofuels. This project developed a new experimental capability to measure important radical intermediates in controlled systems of chemical reactions. This experimental capability is built on optical methods for probing intermediates in high-pressure systems and extends these methods with an application of molecular-beam mass sampling. The interpretation of these systems requires a multiple-scale computational approach combining state-of-the-art detailed theoretical kinetics to rigorously characterize the most important reactions with modeling to capture the global behavior. The results contribute to fundamentally new knowledge base of fuel-structure effects on ignition pathways in poorly characterized but technologically crucial fuels such as ethanol, butanol, cyclohexane (representative of naphthenes, components of

oil-sands-derived fuels) and methyl esters (biodiesel). This knowledge base may provide a foundation for the simultaneous optimization of advanced engines and advanced fuels, an historically unique opportunity afforded by the concurrent revolutions in combustion and fuel technologies.

2. EXPERIMENTAL APPROACHES

The experiments are designed to probe the initial stages of oxidation at elevated pressures. the core of the work has employed an optically-accessible cell based on a University of Göttingen design [3-4]. At the end of the project a second cell was designed and built that will allow molecular-beam mass sampling at elevated pressures.

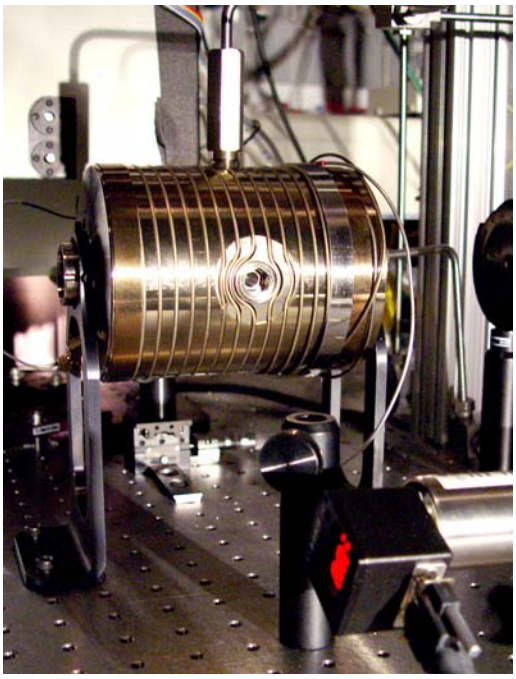

Figure 2. Photograph of high-pressure optically accessible reactor

2.1. Optical Probing of Laser Initiated Oxidation Reactions

The optical probing of photolytically initiated oxidation of fuel species is an outgrowth of earlier work in our group that probed the reactions of alkyl radicals with O_2 at low pressure [5-8]. Whereas the low-pressure experiments used absorption or frequency-modulation probing, the high-pressure experiments used pulsed laser-induced fluorescence (LIF) to follow the course of the pulsed-laser-initiated oxidation.

2.1.1. High-pressure Optical Reactor

The optically accessible reactor must withstand process pressures up to about 100 bar at temperatures up to 1000 K. In addition the included volume should be relatively small, both for safety (reducing stored energy) and to reduce the total flow rate required to refresh the reaction mixture between laser shots. The final design (Figure 2) is taken largely from a reactor designed in the Troe group at the University of Göttingen [4], and is resistively heated by a commercial

heater cable. The cell is constructed from Inconel 718 and has nominal maximum pressure (design MAWP) in excess of 200 bar at 1000 K. Optical access is provided by three fused silica windows sealed by graphite foil into window housings and plugs fabricated from Nimonic 90 alloy. The Nimonic inserts make a metal-to-metal seal against the Inconel 718 cell body.

2.1.2. Using Laser-Initiated Oxidation to Probe Autoignition Reactions

Historically, investigations of fuel structure effects in ignition have tended to concentrate in two areas; the bulk of the studies measure a "high level" marker of ignition efficiency, for example, ignition delay time, and compare to predictions of complex chemical models. The disadvantage of this approach is that, while it may result in a good engineering description of the process under the validated conditions, the lack of information on the fundamental reactions does not permit confidence in predictions outside the experimental validation. On the other hand, elementary chemical kinetics studies are designed to probe single reactions that are critical to the ignition process. These investigations can provide detailed information on the individual reactions being studied, but may fail to recognize other reactions that are important in real ignition. One relatively novel aspect of these experiments is the investigation of reaction systems in the "bridging region" of complexity, where multiple reactions take place, but under sufficiently controlled conditions and with sufficiently detailed measurements of intermediate reactive species that information can be extracted about underlying elementary reaction processes. Initiation of fuel oxidation by laser-photolytic generation of radical species is conducted under conditions where secondary and tertiary reactions can be monitored. The time evolution of radical concentrations reflects a combination of initiation, propagation, branching, and termination reactions. The contributions of these reactions can be changed by changing the concentrations of the reactants and by focusing on different times after the photolytic initiation.

The (substituted) alkyl radicals (R) for the fuels (cyclohexane, ethanol, butanol, 2,5-dimethylfuran, methyl butanoate) were generated by Cl atom reaction of the fuels. The Cl atoms were produced by the pulsed 248 nm photolysis of oxalyl chloride, $(ClCO)_2$.

$$(ClCO)_2 + hv\ (248\ nm) \rightarrow 2Cl + 2CO \qquad (R1)$$

$$RH + Cl \rightarrow R + HCl, \qquad (R2)$$

where RH = fuel, e.g. cyclohexane, ethanol, butanol, propane, 2,5-dimethylfuran, methyl butanoate. All experiments for OH formation were performed using very dilute mixtures of the fuel, oxalyl chloride and oxygen in a large excess of helium. Gas-phase mixtures were prepared in stainless steel vessels at pressures of about 80 bar and allowed to equilibrate for about 24 hours before use. Liquid samples (fuel, oxalyl chloride) were degassed by several freeze-pump-thaw cycles before their vapor was used to prepare the reaction mixtures. Typical concentrations in the reactor were on the order of 10^{16} cm^{-3} fuel, 10^{17} cm^{-3} O_2 and 10^{16} cm^{-3} oxalyl chloride.

The gas temperature in the reactor was determined by thermocouple measurements upstream and downstream of the reaction region and the pressure inside the cell was monitored by a transducer. Total flow rates ensured that the gas sample was completely exchanged for each laser

pulse. About 2-5% of the oxalyl chloride was photolyzed, but the 248 nm absorption of the parent fuel molecules is negligible.

The OH radical is detected by pulsed-laser LIF, excited in the $A(v = 1) \leftarrow X\ (v = 0)$ band at 281.9 nm and detected near 308 nm ($A(v = 1) \rightarrow X\ (v = 1)$ and $A(v = 0) \rightarrow X\ (v = 0)$ emission). The excimer laser used for photolytic initiation and the doubled-dye laser used to excite the OH LIF co-propagate through the cell along the main axis. The OH fluorescence is collected perpendicular to this axis, imaged on the entrance slit of a monochromator which discriminates against scattered 281.9 nm light, and detected with a gated photomultiplier. The probe laser operates at 10 Hz and the photolysis laser at 5 Hz, so that photolysis-on and photolysis-off signals are acquired on alternate probe pulses. The LIF signal is nearly (>90%) saturated, which greatly reduces fluctuations caused by variations in the probe laser intensity.

To record the OH concentration-vs.-time profile, the probe laser delay (relative to the photolysis laser) is varied and the (photolysis-on—photolysis-off) signal is co-added for a number of laser pulses at each time step. To compare the modeled and experimental OH concentrations, the OH LIF signal is calibrated by a reference reaction, the photolysis of an N_2O–H_2O–He mixture at 193 nm. The O (^1D) produced in the photolysis reacts with H_2O to form OH; the water concentration is kept high enough that the reaction of singlet oxygen with other species can be neglected. Molecular oxygen is also added to remove O(^3P). The removal of OH in this system is dominated by the OH + OH reaction, so the concentration of OH can be determined from the measured signal decay and the known rate constant for OH recombination.

2.2. High-Pressure MBMS Reactor

This new approach is designed to overcome the historic inability to measure the critical fuel-based radical species in ignition chemistry, and extend to higher pressure previous successful application of photoionization MBMS to alkyl + O_2 reactions [9-13]. These experiments employ a method pioneered by Gutman and coworkers [14-16], initiating reaction in a slow-flow reactor by pulsed-laser photolysis and following the reaction by mass spectrometric analysis of a nearly-effusive flow out of a small orifice in the side of the reactor. The modification by Osborn and coworkers [12,17] uses photoionization by the tunable vacuum ultraviolet from the Chemical Dynamics Beamline of the Advanced Light Source (ALS) at LBNL. The tunability allows discrimination of isomeric species. The reactor fabricated in this project was designed to operate with the existing mass spectrometer (Figure 3).

The underlying strategy for the design of the high-pressure reactor is simple: the orifice diameter is reduced as the operating pressure is increased in order to maintain a manageable total mass flow rate out of the reactor. A second 3200 L/s turbomolecular pump can also be added to the source chamber (the large chamber in Figure 3). The structure of the reactor cell is based on the design of the optically accessible cell and uses the same window-sealing method. The orifice is laser-drilled in a stainless-steel disk that is welded into an Inconel end-flange (see Figure 4); the orifice size is changed by swapping end flanges. The reactor was completed at the end of the project, and testing and refinement of the apparatus will be carried out under a new project funded by DOE Office of Science.

The considerations for the operation of the high-pressure reactor include ensuring that the photolysis laser fully illuminates the reactor volume, in particular the area adjacent to the sampling orifice. In the present design the photolysis laser in fact impinges on the end flange that contains the sampling orifice, entering from a window on the opposite side. The flow pattern inside the cell is defined by an insert that leads the gases from the inlet to the window side and draws the pump-out from the orifice side. The gas flow is depicted as the black arrows in Figure 4; note that the Autoclave fitting depicted is for a thermocouple and that the gas inlet and outlet are in a different section. This flow permits the gas to be heated as it passes along the outside of the insert (right to left in Figure 4) and then as it flows through the interior section (left to right in Figure 4) allows the maximum residence time for the photolytically excited gas.

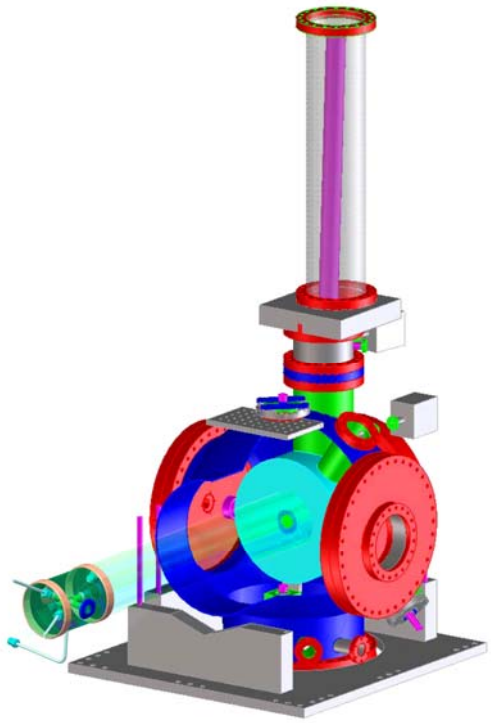

Figure 3. Interface of high-pressure reactor with existing time-of-flight MBMS

The signal levels from high-pressure operation relative to the already operational low-pressure cell are limited by the maximum sustainable pressure in the ionization region and the maximum concentration of target molecules in the reactor. Operationally the maximum ionization region pressure is set by the demands of the microchannel plate detector in the time-of-flight apparatus. The maximum concentration of target molecules in the reactor is set physically by the maximum photolysis density from the laser initiation step, although this bound may in fact be reduced by the need to maintain radical concentrations, and hence reaction rates, low enough to resolve the timescale of the reaction. If one could maintain the same mass flow rate out of the reactor and the same mole fraction of target molecules, the signal levels should be essentially independent of pressure. On the other hand if the target molecule density is fixed then higher pressure implies higher dilution. In this limit the signal *decreases* in inverse proportion to the process pressure. In

practice the response will fall somewhere between these limits; the density in the ionization region will be increased for the same mass flow rate because of the more peaked angular distribution of the supersonic expansion [18]. The improved time fidelity of supersonic sampling [19] may also permit higher densities of target molecules to be used. For example, at 10 bar pressure and 75 μm orifice diameter the speed ratio (the ratio of the beam velocity to the average transverse speed) in the ejected beam should be approximately 20. Under these conditions the experiment could resolve, with the same fidelity, a timescale 30 times shorter than for effusive beam sampling, which could translate into a thirty times greater maximum feasible density of target molecules.

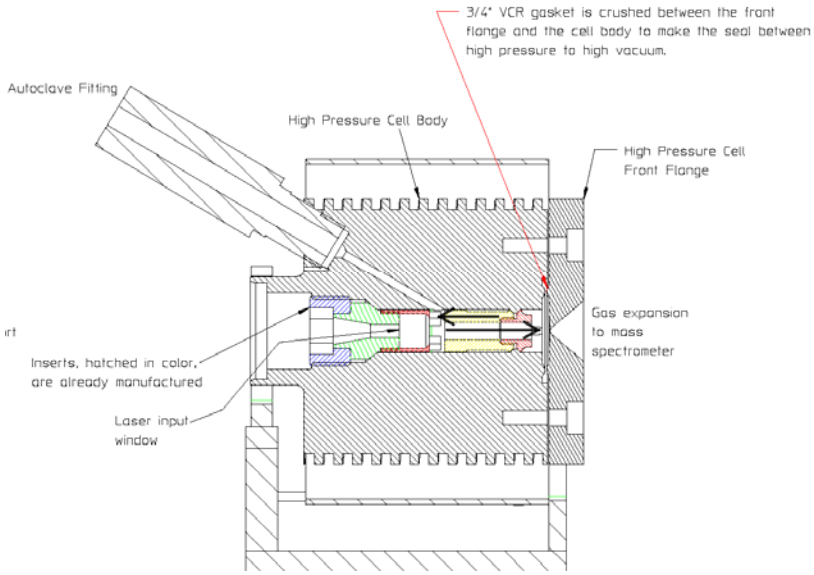

Figure 4. High-pressure MBMS reactor

Other limitations on the operation of the high-pressure MBMS reactor will have to be determined empirically. For example, systems that undergo molecular weight growth could generate particulates that will clog the sampling orifice. Reactions at insufficient dilution or with condensable buffer gases could form clusters in the expansion. It is anticipated that the initial experiments with the high-pressure MBMS will yield many areas for improvement.

[Blank page following section.]

3. COMPUTATIONAL METHODS

The modeling of the experimental profiles was accomplished by a combination of detailed computational kinetics for key reactions and a rate-equation model based on literature rate coefficients for the other reactions in the system. Comprehensive oxidation mechanisms were employed where they were available, but in general these mechanisms were reduced using sensitivity analysis to a much smaller set of reactions that are relevant to the measurements. Detailed calculations were carried out for key reactions in both the cyclohexane and ethanol oxidations. Rate constants for these reactions were computed by solution of the time-dependent multiple-well master equation using the methodology developed by Miller and Klippenstein [20-22]. For barrierless channels such as the initial association of R with O_2 direct variable-reaction-coordinate transition-state theory (VRC-TST) [23-24] was required for accurate rate coefficients. The multiwell ME calculations were carried out with the Variflex programs [25].

For cyclohexane oxidation, the stationary point energies for cyclohexyl + O_2 that were calculated and validated at low pressure by Knepp et al. [8] were employed. For ethanol oxidation the hydroxyethyl + O_2 stationary point geometries were optimized by DFT (B3LYP) calculations using the d,p-polarized split valence 6-311++G(d,p) Gaussian basis set. Accurate energies were computed via RQCISD(T) with the cc-pV*n*Z basis set, n = (T,Q), extrapolated to the infinite basis set limit cc-pV∞Z [26]. However, many stationary points in the hydroxyethyl + O_2 reactions show strong multireference character, in which case energies were calculated using CASPT2 and MRCI with the Davidson correction. If necessary, the geometry was also adjusted by CASPT2/aug-cc-pVDZ calculations. The DFT calculations were performed using the Gaussian 03 suite of programs [27], and other quantum chemical calculations with the MOLPRO package [28].

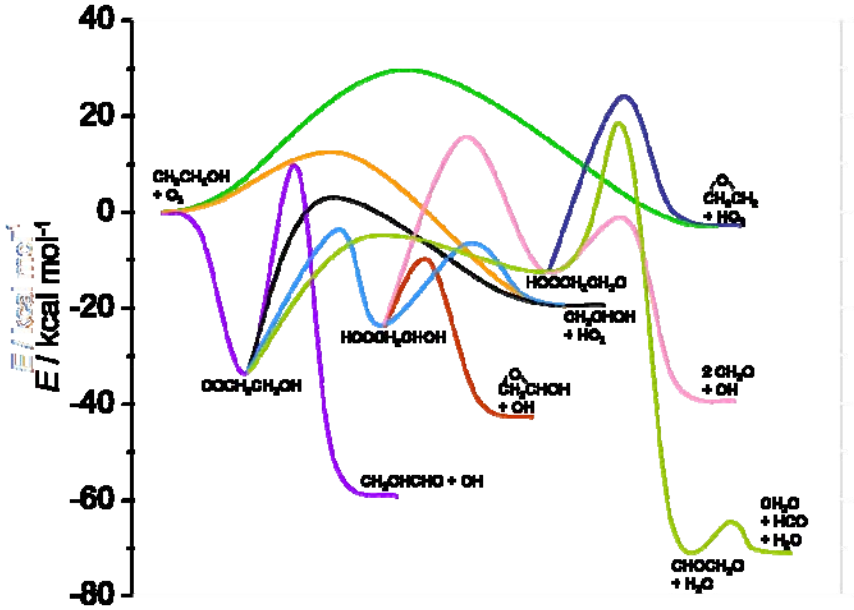

Figure 5. Stationary point energies for the β-hydroxyethyl + O_2 reaction

The potential energy surface for the reaction of β-hydroxyethyl radical with O_2 is shown in Figure 5. The solution to the ME determines the time-dependent populations in all of the wells and products on such a potential energy surface as the reaction progresses and as collisional energy transfer alters the energy distribution of all species. Individual rate coefficients can be derived rigorously from the master equation solution [29]. These rate coefficients include thermal rate constants that transfer population sequentially between adjacent wells, for example, from $OOCH_2CH_2OH$ to $HOOCH_2CH_2O$ or from $HOOCH_2CH_2O$ to OH + 2 CH_2O. However, they also include elementary rate coefficients that transfer population across more than one transition state in a single step, e.g., $OOCH_2CH_2OH \rightarrow$ OH + 2 CH_2O. We refer to these processes as "formally direct" pathways. Chemical activation is one example of such a pathway, where an exothermic reaction leaves a product sufficiently energized to undergo a reaction that would be thermally inaccessible. These pathways exhibit a strong and complex dependence on pressure because collisional energy redistribution alters the branching among the product channels. Typically in combustion models these pathways are neglected and all processes are assumed to be in the high-pressure limit, that is to say, only sequential pathways with thermal rate coefficients participate. The formally direct pathways are kinetically distinguishable in the laser-initiated experiments as well as in the models; they form products on a timescale short relative to that of thermal, sequential product formation. One goal of this program was to determine whether formally direct pathways continue to contribute at the higher pressures relevant to internal combustion engines.

4. FUEL EFFECTS AND PRESSURE-DEPENDENT IGNITION CHEMISTRY

4.1. Oxidation of Cyclohexane

The stationary point energies of the cyclohexyl + O_2 system were characterized and validated by low-pressure experiments. At higher pressures the number of active pathways may be reduced, and a much higher proportion of alkylperoxy and hydroperoxyalkyl radicals will be stabilized than at low pressures. In order to understand these pressure effects, we studied the OH formation in the cyclohexyl + O_2 reaction at higher pressures (6-20 bar) in the temperature range of 586-828 K. The ME based kinetic model of 44 reactions from Knepp et al [8] was adapted to calculate the OH time profiles for the experimentally investigated pressure ranges. The comprehensive mechanism from Silke et al [30] was also used to predict the OH concentration time profiles under our conditions. Fig. 6 below presents the comparison between the experimental results and an *a priori* model. This *a priori* model is constructed by using the Knepp et al. [8] stationary points in a ME equation at high pressure but leaving the rest of the Knepp et al. model unchanged

.

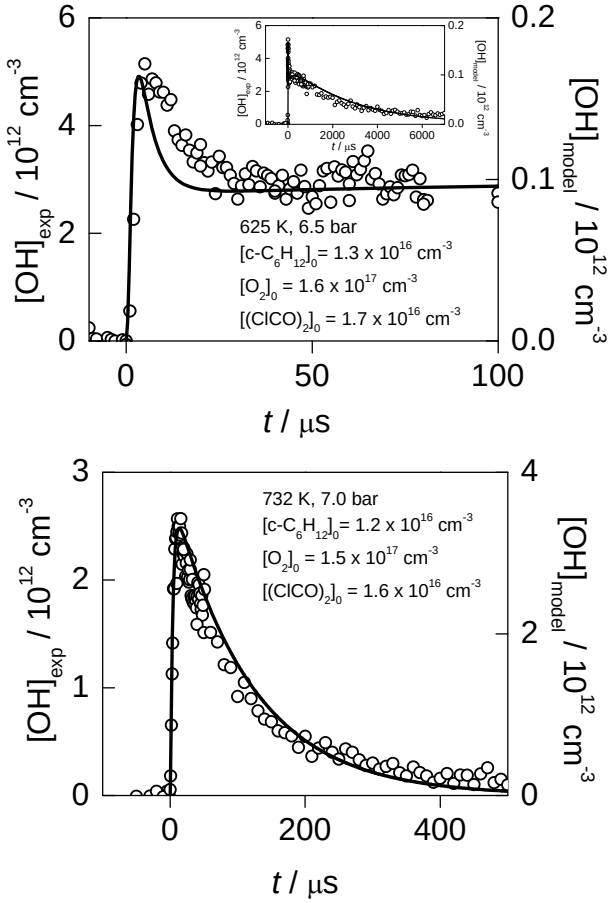

Figure 6. Measured and *a priori* modeled OH concentration-vs.-time profiles from the cyclohexyl + O_2 reaction

The experimental OH time profiles below ~700 K clearly display OH production at two different time scales. Figure 6a (top) shows a sharp peak of prompt OH- formation within the first few μs, followed by sustained OH formation up to about 10 - 15 ms. The *ab initio* model captures the shape of OH formation at both these time scales very well. The relative height of the two peaks as well as the overall decay times of the signals for all temperatures is also very well replicated. However, the model greatly underpredicts the absolute OH concentrations at lower temperatures approximately by factor of 30 and the underprediction decreases at higher temperatures. To investigate the different timescales for OH formation, a detailed rate of production analysis and a sensitivity analysis was performed. The analysis reveals that the short-time OH formation arises from "formally direct paths" even at the highest pressures in our experiments.

To further support this interpretation we calculated the OH concentration with three additional models. In the first all formally direct pathways were eliminated, i.e. rate coefficients connecting nonadjacent wells, reactants or bimolecular products. In the second case a detailed mechanism of Silke et al. [30] was used in an unmodified manner, while in the fourth case a hybrid model was constructed by adding our ME rate coefficients to their model. Results of this are compared in Fig. 7 for 586 K and 7.9 bar.

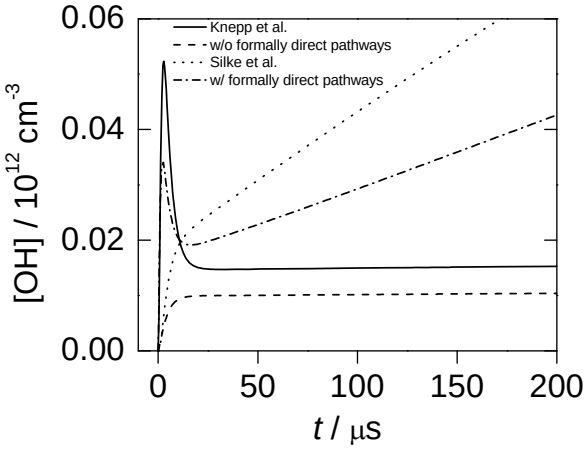

Figure 7. Comparison of the calculated OH concentration-vs.-time profiles at 8 bar and 586 K from different models

Figure 7 shows that exclusion of formally direct pathways results in the removal of the peak at the short timescale for both mechanisms which confirms that prompt OH-formation at low temperatures is a signature for formally direct pathways. The differences in the concentrations between the Silke et al [30] and our model is due to the different level at which secondary chemistry is represented as well as different rate coefficients adopted. Therefore, the observed discrepancy between the two models on the long timescales is not unexpected. At temperatures above 700 K all models predicts a single peak, and the difference between the modified versions of the models is small. At temperatures above 700 K, the OH formation is largely due to the sequential pathways through the isomerization of QOOH from RO_2, which is no longer slow compared to the direct paths. At these temperatures, both the OH producing pathways become indistinguishable resulting in a single OH concentration peak.

Furthermore, the measured discrepancies between the modeled OH concentration and experiments at temperatures below 700 K could be attributed to the second O_2 addition and its subsequent dissociation leading to branching [31].

$$QOOH + O_2 \rightarrow 2\ OH + \text{other products} \qquad \text{(R3)}$$

This hypothetical reaction becomes important only at low temperatures since the thermal decomposition of QOOH above 700 K is sufficiently fast to dominate its removal and that reaction (R3) would have negligible influence on OH concentration at higher temperatures. The inclusion of this reaction in the model gives a good agreement with the experimental and modeled OH profiles, both at low and high pressures [31]; see Figure 8 below. However, it is important to note that reaction R3 is not well studied and the O2QOOH potential energy surface is not well characterized. In fact the general question of the kinetics and products of the second O_2 addition is now the most important unexplained problem in ignition chemistry.

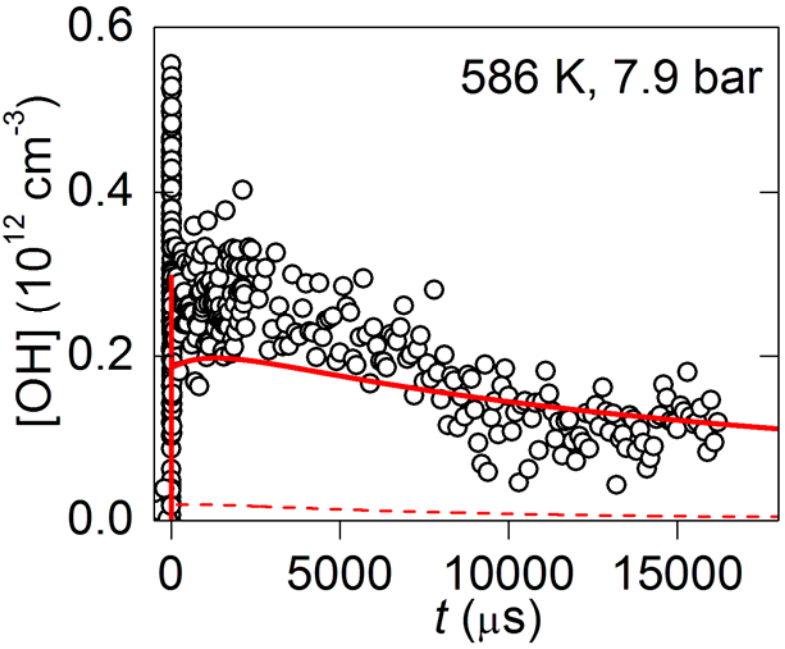

Figure 8. Comparison of the modeled OH concentration-vs.-time profiles from cyclohexane oxidation at 8 bar and 586 K with (solid line) and without (dotted line) addition of a fast QOOH branching reaction

4.2 Oxidation of Ethanol

The oxidation of ethanol was studied in a similar manner as that of cyclohexane. The primary radicals of ethanol are the α-hydroxyethyl (CH_3CHOH) and the β-hydroxyethyl (CH_2CH_2OH) radicals. The subsequent reactions of these radicals with O_2 will govern the initial low-temperature oxidation chemistry:

$$CH_3CHOH + O_2 \rightarrow \text{Products} \qquad \text{(R4)}$$

$CH_2CH_2OH + O_2 \rightarrow$ Products (R5)

As part of this project, detailed potential energy surfaces for reactions R4 and R5 were developed [32]. Both theoretical and experimental work at low pressures indicates that the product of reaction R4 is mainly acetaldehyde + HO_2, while the products of reaction R5 are 2 CH_2O + OH and vinyl alcohol + HO_2. For the kinetics experiments of ethanol oxidation at high pressures, the primary radicals α-hydroxyethyl and the β-hydroxyethyl radicals were generated by the Cl-initiated oxidation of ethanol using reactions R1 and R2. The OH formation is probed using the OH-LIF detection method described above. Fig 3. depicts OH- time profiles at 565 K and 5 bar.

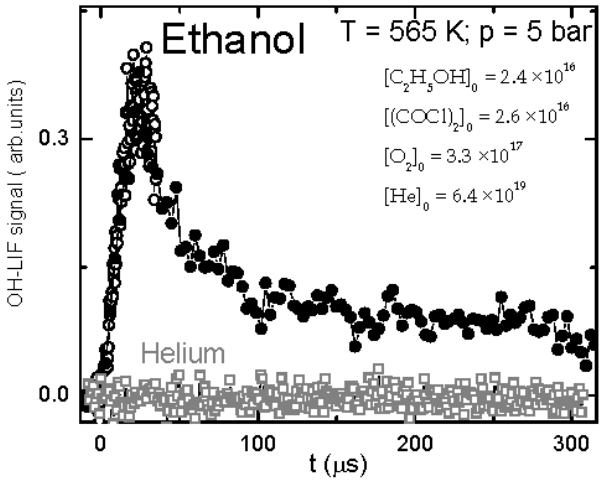

Figure 9. Measured OH formation in ethanol oxidation at 565 K

It is important to note that the OH- formation in ethanol oxidation at lower temperatures does not exhibit the distinctly two different time scales observed in the case of cyclohexane. A combination of detailed theory, computational kinetic modeling and experiments demonstrate that in fact the major source of OH in the low-temperature ethanol oxidation is the reaction of primary radicals with HO_2. This is an extremely interesting development, as the nature of R + HO_2 reactions has not been thoroughly studied under ignition conditions.

4.3. Other Biofuel Oxidation Reactions

In addition to ethanol, we have performed OH-LIF measurements for the oxidation reactions of the primary radicals of butanol, 2,5 dimethylfuran [33] and methyl butanoate. Fig. 10 depicts the OH-formation for butanol and methyl butanoate, with propane oxidation shown for comparison.

The OH formation in case of ethanol (see fig. 9) and *n*-butanol (Fig.10) differs significantly; butanol shows presence of rapid formally direct pathways through a clear bimodal OH-formation profile, whereas ethanol shows no evidence of such paths. However, the prompt OH, the signature of formally direct paths, is substantially less prominent in butanol than seen in the case of cyclohexane discussed earlier.

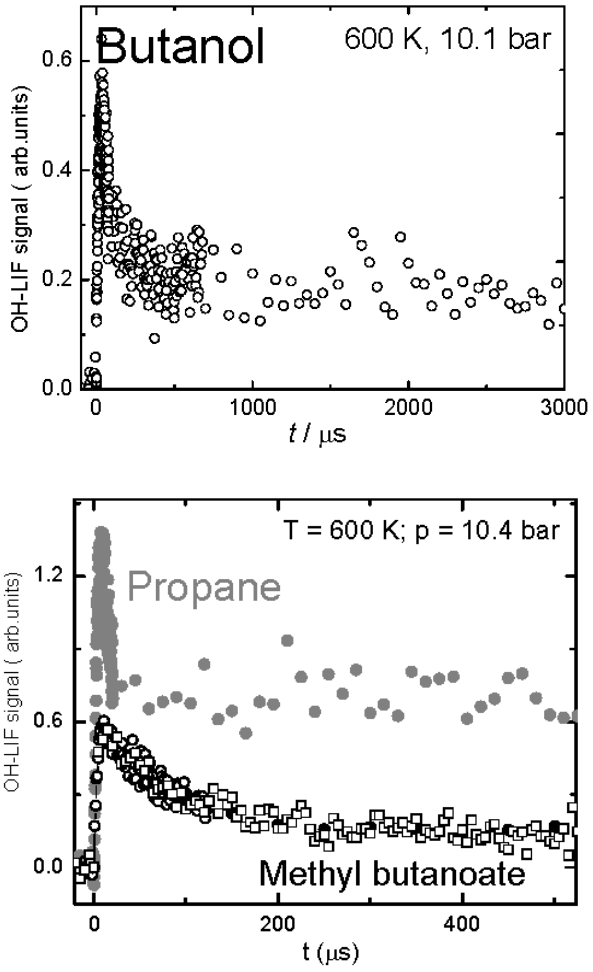

Figure 10. Measured OH formation in butanol and methyl butanoate oxidation at 600 K

Comparison of the OH formation in methyl butanoate (surrogate of biodiesel) oxidation with propane under similar conditions of temperature and pressure and with same initial concentrations shows a complete lack of prompt OH in methyl butanoate but significant prompt OH in the case of propane, which is known to produce OH by formally direct pathways. The 2,5-dimethylfuran oxidation, the other hand does not form *any* detectable OH in the entire temperature and pressure regime investigated in our experiments. The experimental results on OH formation therefore indicate clear fuel dependent chemistry which may change as a function of temperature and pressure. The techniques have also been applied to novel biofuels in an incipient collaboration with JBEI.

[Blank page following section.]

5. CONCLUSIONS

Fundamental chemistry related to autoignition have been measured at elevated pressures for several compounds that are representative of classes of emergent alternative and non-traditional fuels. Modeling of the oxidation was accomplished using a composite of literature-based rate-equation description of most reactions in the system and detailed rigorous computational kinetics of key reactions. The contribution of formally direct reactions is not quenched at conditions relevant to low-temperature heat release in advanced engines, but continues to be significant even up to tens of bar total pressure. Furthermore, at high pressure the chain branching via the reaction of O_2 with QOOH appears to be more prominent than at low pressure, at least for cyclohexane oxidation. Fuel-specific effects on the low-temperature formation of OH have been characterized for a range of biofuel representatives. These experiments have been accomplished in a high-pressure optically accessible reactor, and a new high-pressure MBMS reactor has been constructed that will allow probing of a wider range of species.

6. REFERENCES

[1] H. J. Curran, P. Gaffuri, W. J. Pitz, C. K. Westbrook. A Comprehensive Modeling Study of iso-Octane Oxidation. in *Combust. Flame* vol. 129, pp 253-80, 2002.

[2] E. J. Silke, W. J. Pitz, C. K. Westbrook, M. Sjöberg, J. E. Dec. Understanding the Chemical Effects of Increased Boost Pressure under HCCI Conditions. in *SAE Technical Paper* vol. 2008-01-0019, pp 2008.

[3] R. X. Fernandes, K. Luther, J. Troe. Falloff curves for the reaction CH_3+O_2 (+M) → CH_3O_2 (+M) in the pressure range 2-1000 bar and the temperature range 300-700 K. in *J. Phys. Chem. A* vol. 110, pp 4442-9, 2006.

[4] J. Hahn, *Untersuchungen der Reaktion von Wasserstoffatomen mit Sauerstoffmolekuelen ($H+O_2+M$ => HO_2 +M) in weiten Druck- und Temperaturbereichen*. University of Göttingen, 2004. 101 pp.

[5] E. P. Clifford, J. T. Farrell, J. D. DeSain, C. A. Taatjes. Infrared Frequency-Modulation Probing of Product Formation in Alkyl + O_2 Reactions: I. The Reaction of C_2H_5 with O_2 between 295 and 698 K. in *J. Phys. Chem. A* vol. 104, pp 11549-60, 2000.

[6] J. D. DeSain, E. P. Clifford, C. A. Taatjes. Infrared Frequency-Modulation Probing of Product Formation in Alkyl + O_2 Reactions: II. The Reaction of C_3H_7 with O_2 between 295 and 683 K. in *J. Phys. Chem. A* vol. 105, pp 3205-13, 2001.

[7] J. D. DeSain, S. J. Klippenstein, C. A. Taatjes. Time-resolved measurements of OH and HO_2 product formation in pulsed-photolytic chlorine-atom initiated oxidation of neopentane. in *Phys. Chem. Chem. Phys.* vol. 5, pp 1584-92, 2003.

[8] A. M. Knepp, G. Meloni, L. E. Jusinski, C. A. Taatjes, C. Cavallotti, S. J. Klippenstein. Theory, measurements, and modeling of OH and HO_2 formation in the reaction of cyclohexyl radicals with O_2. in *Phys. Chem. Chem. Phys.* vol. 9, pp 4315-31, 2007.

[9] G. Meloni, T. M. Selby, F. Goulay, S. R. Leone, D. L. Osborn, C. A. Taatjes. Photoionization of 1-alkenylperoxy and alkylperoxy radicals and a general rule for the stability of their cations. in *J. Am. Chem. Soc.* vol. 129, pp 14019-25, 2007.

[10] G. Meloni, T. M. Selby, D. L. Osborn, C. A. Taatjes. Enol Formation and Ring-Opening in OH-Initiated Oxidation of Cycloalkenes. in *J. Phys. Chem. A* vol. 112, pp 13444-51, 2008.

[11] G. Meloni, P. Zou, S. J. Klippenstein, M. Ahmed, S. R. Leone, C. A. Taatjes, D. L. Osborn. Energy-resolved photoionization of alkyl peroxy radicals and the stability of their cations. in *J. Am. Chem. Soc.* vol. 128, pp 13559-67, 2006.

[12] D. L. Osborn, P. Zou, H. Johnsen, C. C. Hayden, C. A. Taatjes, V. D. Knyazev, S. W. North, D. S. Peterka, M. Ahmed, S. R. Leone. The Multiplexed Chemical Kinetic Photoionization Mass Spectrometer: A New Approach for Isomer Resolved Chemical Kinetics. in *Rev. Sci. Instrum.* vol. 79, pp 104103, 2008.

[13] C. A. Taatjes, G. Meloni, T. M. Selby, A. J. Trevitt, D. L. Osborn, C. J. Percival, D. E. Shallcross. Direct Observation of the Gas-Phase Criegee Intermediate (CH_2OO). in *J. Am. Chem. Soc.* vol. 130, pp 11883-5, 2008.

[14] I. R. Slagle, Q. Feng, D. Gutman. Kinetics of the Reaction of Ethyl Radicals with Molecular Oxygen from 294 to 1002 K. in *J. Phys. Chem.* vol. 88, pp 3648-53, 1984.

[15] I. R. Slagle, E. Ratajczak, D. Gutman. Study of the Thermochemistry of the $C_2H_5 + O_2 \leftrightarrow C_2H_5O_2$ and t-$C_4H_9 + O_2 \leftrightarrow$ t-$C_4H_9O_2$ Reactions and of the Trend in the Alkylperoxy Bond Strengths. in *J. Phys. Chem.* vol. 90, pp 402-7, 1986.

[16] I. R. Slagle, F. Yamada, D. Gutman. Kinetics of Free-Radicals Produced by Infrared Multiphoton-Induced Decomposition. 1. Reactions of Allyl Radicals with Nitrogen Dioxide and Bromine. in *J. Am. Chem. Soc* vol. 103, pp 149-53, 1981.
[17] C. A. Taatjes, N. Hansen, D. L. Osborn, K. Kohse-Höinghaus, T. A. Cool, P. R. Westmoreland. "Imaging" combustion chemistry *via* multiplexed synchrotron-photoionization mass spectrometry. in *Phys. Chem. Chem. Phys.* vol. 10, pp 20-34, 2008.
[18] D. R. Miller. Free Jet Sources. In: Scoles G, editor Atomic and Molecular Beam Methods, Oxford: Oxford University Press; 1988, p. 14-53
[19] C. A. Taatjes. How Does the Molecular Velocity Distribution Affect Kinetics Measurements by Time-Resolved Mass Spectrometry? in *Int. J. Chem. Kinet.* vol. 39, pp 565-70, 2007.
[20] J. A. Miller, S. J. Klippenstein. Master Equation Methods in Gas Phase Chemical Kinetics. in *J. Phys. Chem. A* vol. 110, pp 10528 - 44, 2006.
[21] D. K. Hahn, S. J. Klippenstein, J. A. Miller. A theoretical analysis of the reaction between propargyl and molecular oxygen. in *Faraday Discuss.* vol. 119, pp 79-100, 2001.
[22] J. A. Miller, M. J. Pilling, J. Troe. Unravelling Combustion Mechanisms Through a Quantitative Understanding of Elementary Reactions. in *Proc. Combust. Inst.* vol. 30, pp 43-88, 2005.
[23] S. J. Klippenstein. A bond length reaction coordinate for unimolecular reaction. II. Microcanonical and canonical implementation with application to the dissociation of NCNO. in *J. Chem. Phys.* vol. 94, pp 6469-82, 1991.
[24] S. J. Klippenstein. Variational optimizations in the Rice–Ramsperger–Kassel–Marcus theory calculations for unimolecular dissociations with no reverse barrier. in *J. Chem. Phys.* vol. 96, pp 367-72, 1992.
[25] S. J. Klippenstein, A. F. Wagner, R. C. Dunbar, D. M. Wardlaw, S. H. Robertson, J. A. Miller, VARIFLEX, version 1.13m, 2003.
[26] J. M. L. Martin. Ab initio total atomization energies of small molecules - Towards the basis set limit. in *Chem. Phys. Lett.* vol. 269, pp 669-78, 1996.
[27] M. J. Frisch, G. W. Trucks, H. B. Schlegel, G. E. Scuseria, M. A. Robb, J. R. Cheeseman, J. Montgomery, J. A., T. Vreven, K. N. Kudin, J. C. Burant, J. M. Millam, S. S. Iyengar, J. Tomasi, V. Barone, B. Mennucci, M. Cossi, G. Scalmani, N. Rega, G. A. Petersson, H. Nakatsuji, M. Hada, M. Ehara, K. Toyota, R. Fukuda, J. Hasegawa, M. Ishida, T. Nakajima, Y. Honda, O. Kitao, H. Nakai, M. Klene, X. Li, J. E. Knox, H. P. Hratchian, J. B. Cross, C. Adamo, J. Jaramillo, R. Gomperts, R. E. Stratmann, O. Yazyev, A. J. Austin, R. Cammi, C. Pomelli, J. W. Ochterski, P. Y. Ayala, K. Morokuma, G. A. Voth, P. Salvador, J. J. Dannenberg, V. G. Zakrzewski, S. Dapprich, A. D. Daniels, M. C. Strain, O. Farkas, D. K. Malick, A. D. Rabuck, K. Raghavachari, J. B. Foresman, J. V. Ortiz, Q. Cui, A. G. Baboul, S. Clifford, J. Cioslowski, B. B. Stefanov, G. Liu, A. Liashenko, P. Piskorz, I. Komaromi, R. L. Martin, D. J. Fox, T. Keith, M. A. Al-Laham, C. Y. Peng, A. Nanayakkara, M. Challacombe, P. M. W. Gill, B. Johnson, W. Chen, M. W. Wong, C. Gonzalez, J. A. Pople, Gaussian 03, Revision B.01, 2003.
[28] H.-J. Werner, P. J. Knowles, R. Lindh, F. R. Manby, M. Schütz, P. Celani, T. Korona, G. Rauhut, R. D. Amos, A. Bernhardsson, A. Berning, D. L. Cooper, M. J. O. Deegan, A. J. Dobbyn, F. Eckert, C. Hampel, G. Hetzer, A. W. Lloyd, S. J. McNicholas, W. Meyer, M. E. Mura, A. Nicklass, P. Palmieri, R. Pitzer, U. Schumann, H. Stoll, A. J. Stone, R.

Tarroni, T. Thorsteinsson, MOLPRO, a package of ab initio programs version 2006.1, 2006.
[29] S. J. Klippenstein, J. A. Miller. From the Time-Dependent, Multiple-Well Master Equation to Phenomenological Rate Coefficients. in *J. Phys. Chem A* vol. 106, pp 9267-77, 2002.
[30] E. J. Silke, W. J. Pitz, C. K. Westbrook, M. Ribaucour. Detailed Chemical Kinetic Modeling of Cyclohexane Oxidation. in *J. Phys. Chem. A* vol. 111, pp 3761-75, 2007.
[31] R. X. Fernandes, J. Zádor, L. E. Jusinski, J. A. Miller, C. A. Taatjes. Formally direct pathways and low-temperature chain branching in hydrocarbon autoignition: The cyclohexyl + O_2 reaction at high pressure. in *Phys. Chem. Chem. Phys.* vol. 11, pp 1320-7, 2009.
[32] J. Zádor, R. X. Fernandes, Y. Georgievskii, G. Meloni, C. A. Taatjes, J. A. Miller. The reaction of hydroxyethyl radicals with O_2: a theoretical analysis and experimental product study. in *Proc. Combust. Inst.* vol. 32, pp 271-7, 2009.
[33] Y. Román-Leshkov, C. J. Barrett, Z. Y. Liu, J. A. Dumesic. Production of dimethylfuran for liquid fuels: biomass-derived carbohydrates. in *Nature* vol. 447, pp 982-6, 2007.

DISTRIBUTION

1	MS0123	D. Chavez, LDRD Office	1011
2	MS0899	Technical Library	9536
2	MS9018	Central Technical Files	8944


Sandia National Laboratories